Batch-Fabricated Area-Efficient Milli-Actuators

L.-S. Fan, S. J. Woodman, R. C. Moore, L. Crawforth, T. C. Reiley, M. A. Moser

IBM Research Division
Almaden Research Center
650 Harry Road, San Jose, CA 95120-6099

Abstract

We report here a one-mm-sized microfabricated actuator with linearized output capability of 0.2 mN when driven at 60 Volts. This is achieved through an area-efficient design, a high-aspect ratio microfabrication process, and a large signal linearization scheme. The area-efficient design allows full utilization of the chip area for energy conversion. The high-aspect ratio microfabrication process allows the generation of structures an order of magnitude larger than conventional structures in all three dimensions, while still retaining the minimum in-plane features. The large signal linearization scheme permits linearized force output with driving voltages as large as the biasing voltage. This increased output force enables the batch-fabricated microactuators to be used in many new, practical applications in which the microactuators are required to move an additional load, as well as their own mass.

Introduction

Many practical applications, such as attaching microactuators on the back of magnetic recording sliders for improved tracking performance, require that the microactuator move milligram loads at 10's of G's of acceleration. For dynamic performance, it is also important that any nonlinearity in the device be minor to permit the closing of a high bandwidth feedback loop. Achieving this goal requires a linearized driving force of a few hundreds μN generated in a mm-sized area. This requirement on the linearized force output from the microactuator is four orders of magnitude larger than the conventional force output from a typical polysilicon device. Here, we will show how one can achieve the goal through an area-efficient design, a high-aspect ratio microfabrication process, and a large signal linearization scheme.

Area-efficient Electrostatic Microactuators

In addition to the achievable energy density, the effectiveness of an actuator will depend on how efficiently the device utilizes the chip area for energy conversion, along with other constraints such as position independent output, stroke range etc.. Constant in-plane force in the mN range, with a few μm of stroke can be generated in a microfabricated electrostatic structure assuming full utilization of the available area such as the electrical tree structure [1-2] shown in Fig. 1. In this approach, energy conversion cells populate the whole area and efficiently convert electrical energy into force or torque. The electrodes in Fig. 1 are grouped into three sets, each with three levels of hierarchy: trunk, branch, leaf. Each level branches out from a higher level, and the scheme

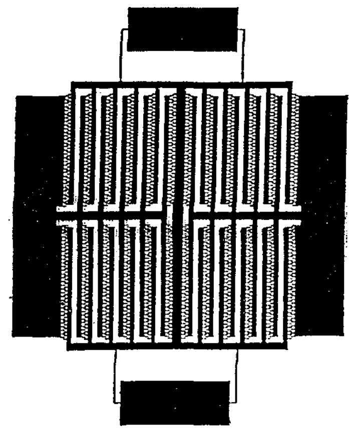

Figure 1. Top View of an area-efficient electrode tree structure with the air gaps between electrodes being less than 2 μm.

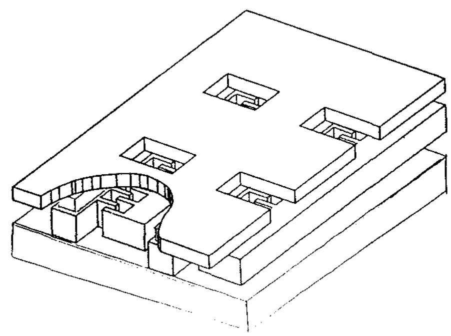

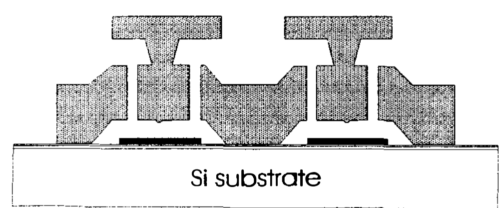

Figure 2. Perspective and cross sectional view of the area efficient actuator with a bonding platform connecting all of the movable electrodes on top.

can be recursively extended if needed. The electrodes are layout such that only one masking level is needed to define the electrode sets that can generate position-independent electrostatic force in both direction. A bonding platform covering most of the area is formed on top of the electrode. It is used to connect all the movable electrodes and also acts as the platform for payload attachment. A stud layer is used to elevate the bonding platform to a certain height above the stator electrodes; this height depends on the vertical electrical field component and spring stiffness. Figure 2 shows the perspective view and cross setion of an area-efficient actuator.

Device Processing

The force output of the interdigitated microactuator is proportional to the height-to-width aspect ratio of the gaps between fingers, and this requires a high-aspect-ratio fabrication process. [4-7] To achieve this and to maximize the stiffness/mechanical bandwidth aspect of the device, we reported earlier [2] a process capable of fabricating 20 μm thick microminiature metal structures with minimum features sizes less than 2 μm. This added structure height and associated rigidity has enabled us to fabricate structures with in-plane dimensions of a few millimeters using a low-stress, plated copper. The structures have dimensions an order of magnitude larger than conventional micromechanical structures in all three dimensions, while still retaining the minimum in-plane features. This is achieved by using a combination of very low-stress plating, photoresist and a projection optical system. Here, we have extended the process to allow the microfabrication of an area-efficient electrode tree structure as proposed in [1], based on a flexure type of actuator [3]. For the electrostatic devices, copper is used, which is compatible with the PSG (phosphor-silicate glass)-HF sacrificial layer system, thereby minimumizing the process changes of the conventional silicon-based surface micromachining. Since plating is a low temperature process, this silicon-based technology could potentially be merged with on-chip silicon control and sensing circuitry. Fig. 3 outlines the fabrication sequence of the device. The Si wafer is first oxidized at 1050° C, and followed by deposition of LPCVD silicon nitride as a passivation layer. An LPCVD polysilicon shield layer is deposited and patterned by CCl_4 plasma etching. An LPCVD PSG sacrificial layer is deposited at 450° C and patterned by wet etch in BHF. Recessed holes are time-etched into the PSG layer to form molds for dimples. A full-film chromium and copper composite layer (Cr 100 Å and Cu 900 Å thick) is sputtered onto wafers as a plating seed layer. A plating stencil is formed by a patterned 22-μm-thick photoresist layer. The edges of the wafers are exposed to UV to form a contact ring of seed layer which is then contacted to the plating electrode during the Cu plating. The plated copper is twenty μm thick, and a 2-μm margin on the photoresist is left for the plating nonuniformity to avoid plating mushroom over the photoresist. This is necessary to avoid shunting of the interdigitated electrodes which are only 2 μm apart. The intrinsic stress level of the plated copper layer is as low as 20 MPa. A copper bonding platform connecting all of the movable electrodes on top is formed in two other similar plating steps for structural rigidity and payload attachment, and the actuators are finally released in an HF based etchant. A supercritical CO_2 drying release process [8] is used. The final

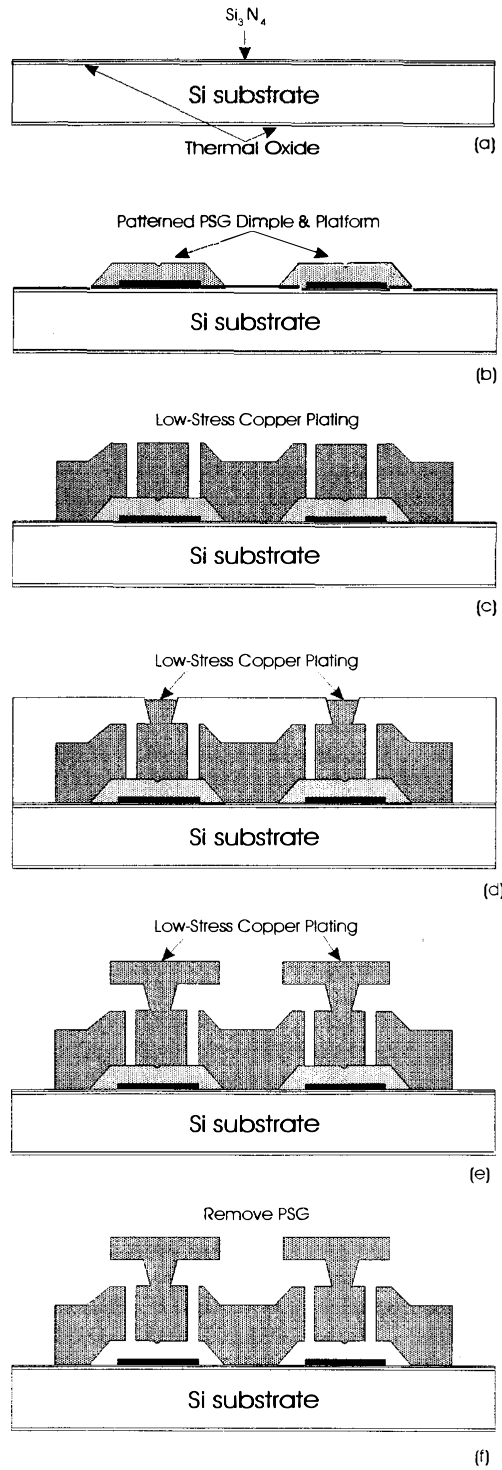

Figure 3. Outline of device fabrication sequence. (a) substrate is isolated (b) first conducting layer and sacrificial layer are patterned (c) high-aspect-ratio stencil plating (d) pedestal plating (e) bonding platform plating (e) release process.

released structures are shown in the SEM micrographs in Fig. 4 and Fig. 5 with and without the bonding platform.

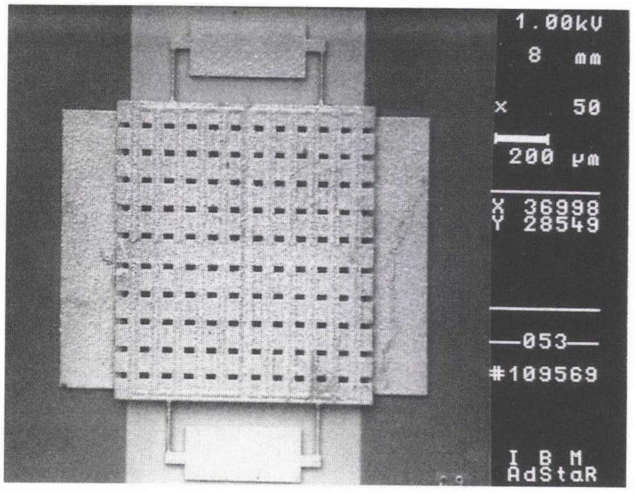

Figure 4. SEM micrograph of a released area-efficient microactuator.

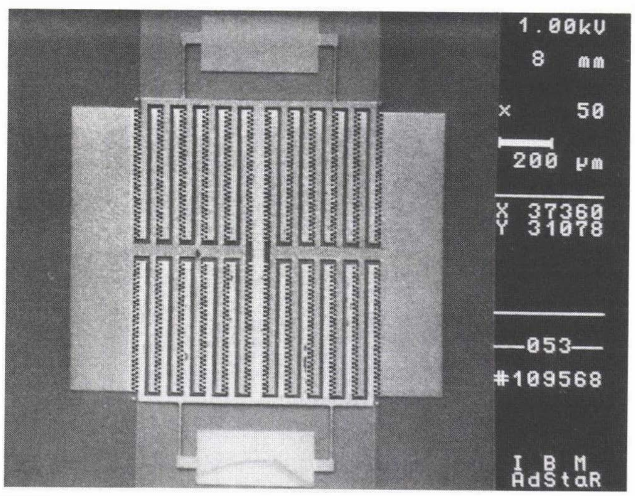

Figure 5. SEM micrograph of an area-efficient actuator with the bonding platform removed to expose the electrode tree structure.

Large signal linearization

Electrostatic actuators are square law devices. Although the force is independent of position within the designed stroke range for interdigitated electrode configurations, the force/acceleration is proportional to the square of the applied voltage between the moving electrode and stator electrode. Linearization becomes an important issue for this category of electrostatic actuator control. A typical linearization scheme is to sum a small control voltage to a large DC biasing voltage, and the quadratic nonlinearity in the control signal can be ignored for large bias voltages [2],[4]. Although the electrical driving force is linearized in the scheme,

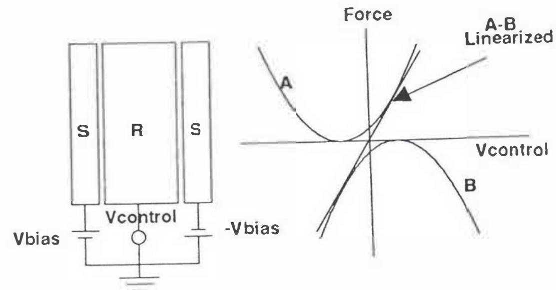

Figure 6. (a) Large signal linearization scheme with an anti-symmetrical bias on the stators (b) Nonlinearity is cancelled out, and the output is linearized with driving voltages as large as the biasing voltage.

the spring stiffness becomes asymmetric if the DC bias causes large initial displacement. Finally, the linearity scheme breaks down when the "small signal" voltage is nearly as large as the DC bias voltage. In practical servo applications, one would need the actuator to generate as large a force or torque as possible by putting in the maximum allowable signal while still maintaining system linearity. In order to drive the device in a large signal linearized mode, a new linearization bias configuration is used as shown in Fig. 6(a). The force/input relation becomes

$$F_{el} = \alpha_1(V_{bias} + V_{control})^2 - \alpha_2(V_{bias} - V_{control})^2$$
$$= 4\alpha V_{bias}V_{control},$$

where α_1 and α_2 are force constants of the two sides, here set equal to α.

The amplitude of the control signal can be equal to or even larger than the large DC bias and still maintain the linear relation in this configuration, and the optimum bias and maximum control signal should both be one half of the maximum allowable voltage for the system. Fig. 6(b) shows how two segments of the transfer curves are put together for a linearized curve. Also, there is no initial displacement and the initial spring stiffness is symmetric in this case. Certainly, this scheme depends on good process tolerance control and the symmetry of this particular device in order to satisfy the condition that α_1 equals α_2.

Microactuator Characteristics

A Laser Doppler Velocimeter (LDV) was used to measure the in-plane motion. The frequency response function is measured on the system using the control voltage as an excitation and the LDV displacement as a response. The dominant resonance is at 9 kHz as shown in Fig. 7. Fig. 7 also shows the phase response with a clean 180 degrees transition after first resonance. We showed in earlier paper [2] that a significant reduction in the peaking amplitude response can be achieved in this kind of actuator using a PI controller [9].

The output force of microactuators can be obtained from the measured amplitude of acceleration when sinusoidal excitations at frequencies significantly higher than the first resonance are used. Fig. 8 shows the acceleration per volt

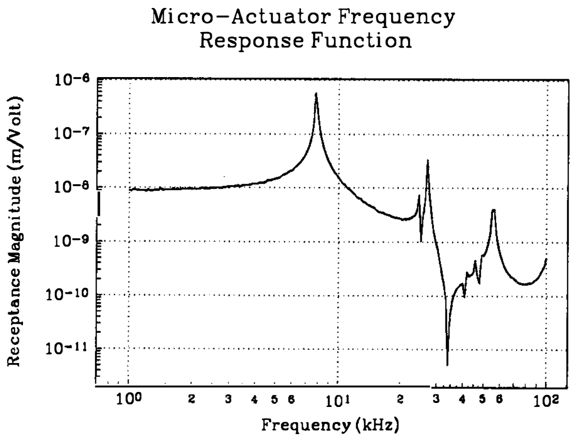

Figure 7. Amplitude and phase of microactuator frequency response function up to 100kHz.

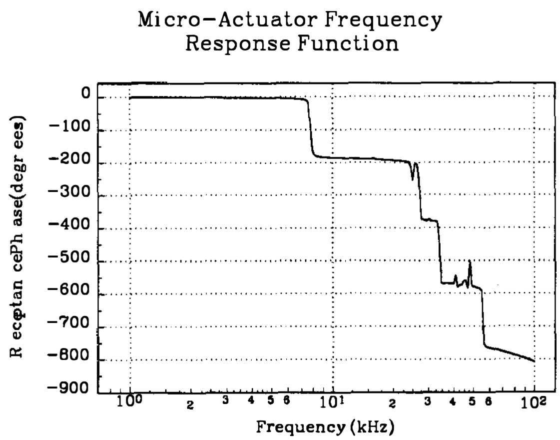

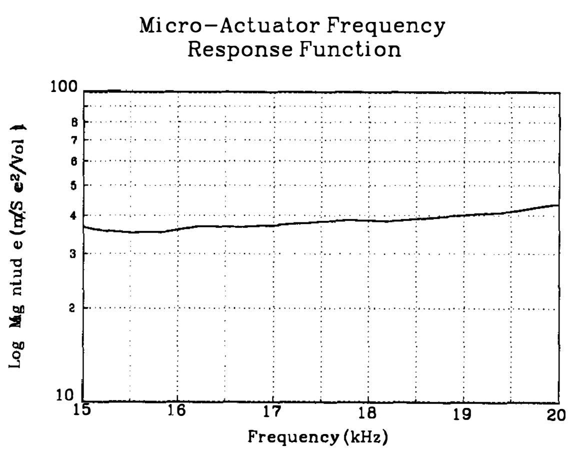

Figure 8. Acceleration per volt of a sinusoidal driving voltage for an area-efficient actuator biased at 30 volts.

of a sinusoidal driving voltage from 15 to 20 kHz for an actuator biased at 30 Volts. Given a movable electrode mass of 45 μg, a force output of $6x10^{-8}N/V^2$ is obtained; i.e., a linearized force output of 0.2 mN can be obtained from this one-mm-sized microactuator at 60 Volts, which is a feasible voltage generated on a modified CMOS chip.

To verify the linearity, the actuator was driven with a sinusoidal excitation well below the first resonant frequency to ensure a zero phase shift. Fig. 9 shows the actuator displacement in the time domain, while driven by a large signal sinusoidal wave at 5 KHz, which is below the resonant frequency. It shows that the actuator tracks the input signal. The input amplitude is 20 V in this case, and the displacement versus input curve is plotted in Fig. 10. Good linearity is obtained and no hysteresis is observed, compared to typical piezoelectric or magnetic approaches where the linearity will greatly depend on the material characteristics used for transduction in additional to possible flexure nonlinearity.

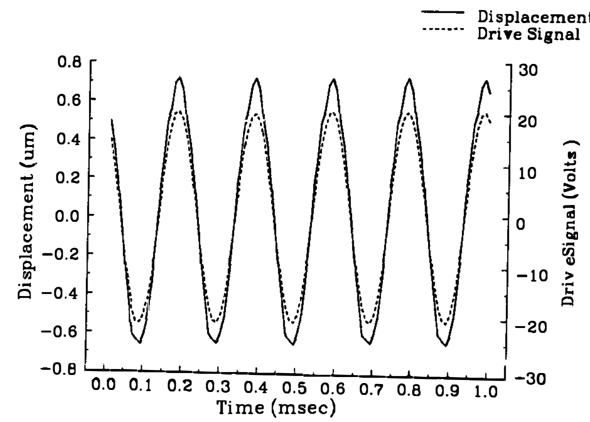

Figure 9. Actuator displacement driven by a 5 kHz sinusoidal excitation shows the actuator output tracks the input signal.

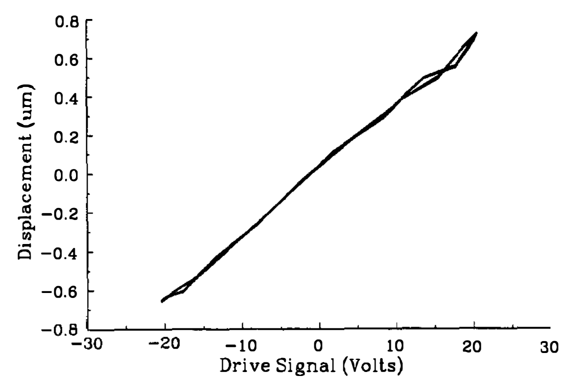

Figure 10. Displacement vs. input curve using the large signal linearization scheme.

Area-Efficient Rotary Microactuators

A consideration with the in-plane linear microactuators is that the force generated does not necessary pass through the center of mass (C.M.) of the combined mass of payload and movable electrode. Thus, one needs to take the cross-axis torque into consideration in a practical system design. A rotary version of the area-efficient actuator such as shown in Fig. 11 (with upper bonding plate not shown) will reduce this complication. Since the rotational axis passes through the center of mass of the movable electrode in this symmetric design, a centered payload will make the combined system C.M. on the axis of rotation.

Another consideration with linear microactuators is that shock loads applied in the direction of motion lead to displacements of the actuator. The displacement may be sufficient to disrupt successful operation during high G shocks. A rotary version of the area-efficient actuator will also greatly reduce the shock sensitivity. The same area-efficient process described above is used to fabricate such a device. Fig. 11 shows an SEM photograph of a microfabricated area-efficient rotary microactuator. The springs are designed such that they provide a sufficiently low torsional spring constant to allow rapid in-plane rotation under the electrostatic forces available, and sufficiently high load bearing capability to accommodate shock loads. One handy way to achieve low rotational stiffness while maintaining the same out-of-plane stiffness is to split a spring into several ones as shown in Figure 12. This is because the vertical stiffness is linearly proportional to the width of the spring, but the in-plane bending stiffness is proportional to the cube of the thickness in the bending direction. For certain applications a rotary version of area-efficient design may have advantageous shock resistance and reduced cross-axis mechanical coupling.

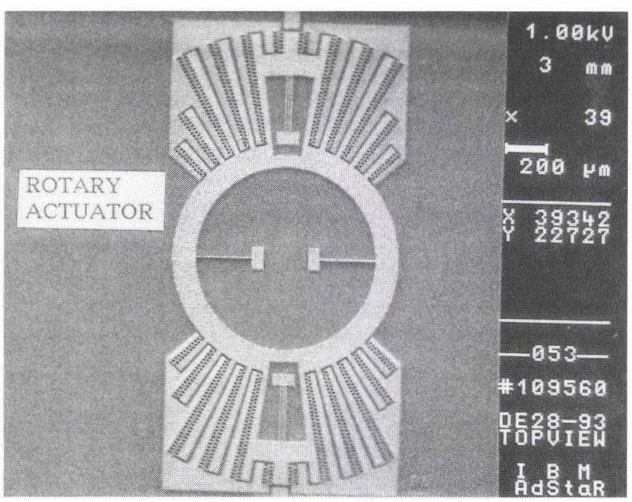

Figure 11. SEM micrograph of an area-efficient rotary actuator. (without the bonding platform)

Summary

We have described the design, process and characteristics of area-efficient microfabricated actuators. Through an area-efficient design, a high-aspect ratio microfabrication process, and a large signal linearization scheme, we have shown that a one-mm-sized microfabricated actuator is capable of linearized output of 0.2 mN when driven at 60 Volts. The compactness, the linearity and the increased output force/torque may enable the batch-fabricated microactuators to be used in many practical and new applications such as slider tracking in magnetic recording, optical tracking, non-resonant mode scanning/chopping, optical frequency domain demultiplexing with a tunable external Fabry-Perot cavity etc.. A design for a rotary microactuator was shown, and some of its potential advantages given.

Acknowledgment

The authors want to acknowledge L. H. Lane, S. Hoen, D. D. Tang, H. Santini, H. Levinson for valuable inputs and support.

References

[1] L. S. Fan, "Towards mN electro-and magneto-static microactuators." Proceedings of the Workshop on Microtechnologies and Applications to Space Systems, NASA, 191-192 (June 1993)

[2] L.-S. Fan, L. H. Lane, N. Robertson, L. Crawforth, M. A. Moser, T. C. Reiley, W. Imaino, "Batch-fabricated milli--actuators", Proceedings of IEEE ASME Micro Electro Mechanical System, 179-183 (Feb. 1993)

[3] W. C. Tang, T. C. H. Nguyen, R. T. Howe, "Laterally driven polysilicon resonant microstructures", Sensors and Actuators, Vol. 20 25-32 (1989)

[4] W. Becker, W. Ehrfeld, P. Hagmann, A. Maner and D. Munchmeyer, "Fabrication of microstructures with high aspect ratios and great structural heights by synchrotron radiation lithography, galvanoforming, and plastic moulding (LIGA process)", Microelectronic Engineering 4 (1986) 35-56.

[5] H. Guckel, T. R. Christenson, K. J. Skrobis, D. D. Denton, B. Choi, E. G. Lovell, J. W. Lee, S. S. Bajikar and T. W. Chapman, "Deep X-Ray and UV lithographies for micromechanics", Proc. of the IEEE Solid-State Sensor and Actuator Workshop, Hilton Head, SC, (1990) 118-122.

[6] A. B. Frazier, M. G. Allen, "High aspect ratio electroplated microstructures using a photosensitive polyimide process", Proc. IEEE MEMS'92 workshop, Travemunde, Germany (1992) 97-102

[7] G. Engelmann, O. Ehrmann, J. Simon, H. Reichl, "Fabrication of high depth-to-width aspect ratio microstructures", Proc. IEEE MEMS'92 workshop, Travemunde, Germany (1992)

[8] G. T. Mulhern, D. S. Soane, R. T. Howe, "Supercritical carbon dioxide drying of microstructures", Digest of Technical Papers, International Conference on Solid-State Sensors and Actuators, 296-298, Yokohama, Japan, (1993)

[9] R. C. Dorf, Modern Control Systems, Third Edition, Addison-Wesley Publishing Co., Reading, MA, 1980.